

Selective Activation of C-OH, C-O-C, or C=C in Furfuryl Alcohol by Engineered Pt Sites Supported on Layered Double Oxides

Yanru Zhu, Wenfang Zhao, Jian Zhang, Zhe An, Xiaodan Ma, Zhijun Zhang, Yitao Jiang, Lirong Zheng, Xin Shu, Hongyan Song, Xu Xiang, and Jing He

ACS Catal., **Just Accepted Manuscript** • DOI: 10.1021/acscatal.0c01276 • Publication Date (Web): 29 Jun 2020

Downloaded from pubs.acs.org on June 29, 2020

Just Accepted

“Just Accepted” manuscripts have been peer-reviewed and accepted for publication. They are posted online prior to technical editing, formatting for publication and author proofing. The American Chemical Society provides “Just Accepted” as a service to the research community to expedite the dissemination of scientific material as soon as possible after acceptance. “Just Accepted” manuscripts appear in full in PDF format accompanied by an HTML abstract. “Just Accepted” manuscripts have been fully peer reviewed, but should not be considered the official version of record. They are citable by the Digital Object Identifier (DOI®). “Just Accepted” is an optional service offered to authors. Therefore, the “Just Accepted” Web site may not include all articles that will be published in the journal. After a manuscript is technically edited and formatted, it will be removed from the “Just Accepted” Web site and published as an ASAP article. Note that technical editing may introduce minor changes to the manuscript text and/or graphics which could affect content, and all legal disclaimers and ethical guidelines that apply to the journal pertain. ACS cannot be held responsible for errors or consequences arising from the use of information contained in these “Just Accepted” manuscripts.

1
2
3
4
5
6
7
8
9
10
11
12
13
14
15
16
17
18
19
20
21
22
23
24
25

Selective Activation of C-OH, C-O-C, or C=C in Furfuryl Alcohol by Engineered Pt Sites Supported on Layered Double Oxides

26
27
28
29
30
31
32
33
34
35
36
37
38

*Yanru Zhu,[†] Wenfang Zhao,[†] Jian Zhang,[†] Zhe An,[†] Xiaodan Ma,[†] Zhijun Zhang,[†] Yitao Jiang,[†]
Lirong Zheng,^{*,§} Xin Shu,[†] Hongyan Song,[†] Xu Xiang,[†] and Jing He^{*,†}*

39
40
41
42
43
44
45
46
47
48
49
50
51
52
53
54
55
56
57
58
59
60

[†] State Key Laboratory of Chemical Resource Engineering & Beijing Advanced Innovation
Center for Soft Matter Science and Engineering, Beijing University of Chemical Technology,
Beijing 100029, P. R. China

[§] Institute of High Energy Physics, the Chinese Academy of Sciences, Beijing 100049, P. R.
China

KEYWORDS: Atomic Pt, 2D Pt cluster, 3D Pt cluster, hydrogenation of furfuryl alcohol,
selective activation

ABSTRACT

The selective activation of targeted bonds in biomass-derived furfural or furfuryl alcohol with complex chemical linkages (C-C/C-H/C-O, C=C/C=O, or C-O-H/C-O-C) is of great challenge for biomass upgrading, expecting well-defined catalyst and definite catalytically active sites. This work demonstrates an efficient targeted activation to C-OH, C-O-C, or C=C by engineering the structure of catalytic Pt sites, affording 2-methylfuran (2-MF), tetrahydrofurfuryl alcohol (THFA), or 1,2-pentanediol (1,2-PeD) as product in the hydroconversion of furfuryl alcohol. The catalytic Pt sites have been engineered as atomic Pt, coordination unsaturated Pt-Pt in atom-thick dispersion, or coordination unsaturated 3D Pt-Pt by tailoring the Pt dispersion (single atom, 2D cluster, or 3D cluster) on Mg and Al-containing layered double oxide (Mg(Al)O) support. The selective activation of C-OH, C-O-C, or C=C has been traced with the FT-IR spectra recorded surface reaction. On atomic Pt, C-O-H is easily activated, with the assistance of Mg(Al)O support, with O-terminal adsorption without affecting furan C-O and C=C. But C=C in furan ring is easier to be activated on coordination-unsaturated Pt-Pt in atom-thick dispersion, resulting in a step-by-step hydrogenation to generate THFA. On coordination-unsaturated 3D Pt-Pt, the hydrogenolysis of furan ring is favored, resulting in the cleavage of furan C-O to produce 1,2-PeD. And that, the Mg(Al)O supports derived from Mg and Al layered double hydroxides (LDHs) here also play a key role in promoting the selectivity to 1,2-PeD by providing basic sites.

1. Introduction

The catalytic conversion of biomass as well as biomass-derived platform molecules to fuels and value-added chemicals has been attracting wide attention for the development of sustainable chemical industry.¹⁻³ Furfuryl alcohol are promising C₅ biomass-derived molecule produced by hydrolysis and dehydration of hemicellulose,^{4,5} and has already been manufactured from furfural in a commercial scale.⁵ Selective hydrogenation and hydrogenolysis are considered to be the most effective methods for conversion of furfural/furfuryl alcohol to valuable chemicals.⁶⁻⁸ 1,2-pentanediol (1,2-PeD)⁹⁻¹² or 1,5-pentanediol (1,5-PeD)¹³⁻¹⁵, the most valuable products used as monomers of resins, has been produced by the selective ring-open. 2-Methylfuran (2-MF), a potential fuel or fuel additive, has been generated by the selective hydrogenolysis of C-OH.^{16,17} Tetrahydrofurfuryl alcohol (THFA), used as a green solvent, has been formed by the C=C hydrogenation.^{18,19} The complexity of chemical linkages (C-C/C-H/C-O, C=C/C=O, C-O-H/C-O-C, etc.) in furfural/furfuryl alcohol molecules provides great chance to produce various high value-added chemicals or fuels, but at the same time makes the selective activation of targeted bonds much more challenging.⁶ And that, the hydroconversion of furfural/furfuryl alcohol usually involves multiple competitive reactions, leading to a low selectivity to target product.²⁰

Supported noble metals (Pt, Ru, Ir, Pd etc.), transition metals (Cu, Ni, etc.), or complex components have been developed for the hydroconversion of furfural/furfuryl alcohol.²⁰⁻²² Hydrotalcite-supported Pt nanoparticles efficiently catalyze the direct hydrogenolysis of furfural to 1,2-PeD with a selectivity of 73 % and a conversion of 99 %.²³ Furfuryl alcohol is completely transformed to THFA on ultrafine SiO₂-MOF supported NiCo alloy, giving 99.1 % selectivity of THFA.¹⁹ In the gas-phase hydrogenation of furfural, Pt-Fe particles supported on SiO₂ exhibit a 2-MF selectivity of 63 % with good stability.²⁴ The adsorption mode of furanic compounds and

1
2
3 the activation of specific chemical bond not only highly depend on the nature of metals and the
4 catalyst composition but also are sensitive to the microstructures of catalysts and the structures of
5 catalytically active sites.²⁰⁻³⁴ TiO₂ supported atomic Ir exhibits superior conversion and
6 selectivity of C₃N₄ supported atomic Ir in the hydrogenation of furfural to furfuryl alcohol,
7 attributed to the appropriate strength of interactions between the active metal sites and the
8 reactant molecules owing to the regulation of the support materials.²⁶ The selectivity to 1,5-
9 pentanediol from furfuryl alcohol hydrogenolysis increases with increasing TiO_y layer thickness
10 covered on TiO₂-supported Co particles.²⁷ Bimetallic Cu-Ni supported on TiO₂, with surface Cu-
11 rich structures, allows for high selectivity to 2-MF or 2,5-dimethylfuran from furfural or 5-
12 hydroxymethylfurfural.²⁸ Formation of Ir-Rh alloy and modification of ReO_x species on Ir-Rh
13 alloy particles enhance the hydrogenation activity of furfural to THFA.²⁹ The sensitivity of
14 catalytic activity and/or selectivity to the structure of active sites has been observed in nano-
15 catalyzed biomass conversion.^{25,27,30-34} In the hydrogenation of furfural, a selectivity of 97 % to
16 furfuryl alcohol has been achieved on steps/edges-rich Ni nanoparticles by facilitating the
17 exclusive activation of HC=O group, while a selectivity of 99 % to THFA is produced on a high
18 exposure of Ni (111) plane by the activation of both furan ring and C=O group.³⁰ The selective
19 α -C-O cleavage in 2-furancarboxylic acid hydrogenolysis to synthesize 5-hydroxyvaleric acid
20 has been achieved on Pt particles with low-index Pt surface (111 plane) at a low temperature of
21 313 K.³¹ In the vapor-phase hydrogenation of furfural,³² product selectivity changes as function
22 of size and shape of Pt nanoparticles. Upon an increase in Pt particle size from 1.5 to 7.1 nm, the
23 selectivity toward furfuryl alcohol increases from 1 % to 66 %, and the furfuryl alcohol
24 formation rate increases from 0.001 s⁻¹ to 0.076 s⁻¹.³² Furfuryl alcohol or THFA has been
25 produced depending on the size of Pd nanoparticles.³³ In addition to particle size, chemical states
26
27
28
29
30
31
32
33
34
35
36
37
38
39
40
41
42
43
44
45
46
47
48
49
50
51
52
53
54
55
56
57
58
59
60

1
2
3 of metal sites usually inherently affect the adsorption and activation behavior in catalysis.³⁴
4
5 Tuning the chemical state of supported Pt species by varying the exposed lattice-planes of CeO₂
6
7 support, leads to significantly different selectivity to 1,2-PeD in the hydrogenolysis of furfuryl
8
9 alcohol.³⁴
10

11
12 The effects of metal dispersion, from nanoparticles to single atoms, have been reported for a
13
14 variety of industrially promising or important reactions.³⁵⁻³⁷ The sensitivity of chemical bond
15
16 activation to metal dispersion is highly desired for the conversion of biomass and/or biomass-
17
18 derived molecules. This work demonstrates the dependence of chemical bond activation in the
19
20 conversion of biomass to the structure nature of metal sites, from single atoms to nanoclusters. Pt
21
22 sites has been tuned here as dispersed in single atoms, coordination unsaturated 2D clusters, and
23
24 coordination unsaturated 3D clusters on Mg and Al-containing layered double oxide (Mg(Al)O),
25
26 and the targeted activation to C-OH, C-O-C, or C=C has been investigated. 2-MF, 1,2-PeD, or
27
28 THFA has been produced as a result of targeted activation of C-OH, ring C-O-C, or ring C=C in
29
30 the hydroconversion of furfuryl alcohol.
31
32
33
34
35
36
37
38
39
40
41
42
43
44
45
46
47
48
49
50
51
52
53
54
55
56
57
58
59
60

2. Results and Discussion

The Mg(Al)O supported Pt investigated in this work results from the reduction of Pt²⁺-loaded layered double hydroxides (LDHs). The Mg and Al-containing LDHs (MgAl-LDHs) was first synthesized in-situ on the surface of γ -Al₂O₃ by a method reported previously by our group^{38,39} (denoted MgAl-LDHs@Al₂O₃), and then [Pt(NH₃)₄]²⁺ was loaded as Pt source. In the X-ray diffraction (XRD) patterns (Figure S1), the reflections characteristic of hydrotalcite structure and γ -Al₂O₃ are clearly observed for MgAl-LDHs@Al₂O₃. From the scanning electron microscopic (SEM) images (Figure S2), MgAl-LDHs is observed to grow vertically on both exterior and interior surfaces of Al₂O₃ spheres with a thickness of \sim 1.15 μ m. By varying the concentration of Pt²⁺ aqueous solution for incipient-wetness impregnation, Pt²⁺/MgAl-LDHs@Al₂O₃ with input Pt²⁺ loading of 0.10 wt%, 0.15 wt%, 0.78 wt%, or 1.80 wt% was prepared. No visible change is observed in the XRD patterns (Figure S1) after Pt loading. By the in situ reduction (thermal treatment in H₂) of Pt²⁺/MgAl-LDHs@Al₂O₃ at 400 °C, Mg and Al-containing layered double oxides (Mg(Al)O) supported Pt (Pt/Mg(Al)O@Al₂O₃-IR) was produced. No Pt phase can be observed (Figure S3 a-d) in each reduced sample, indicative of well-dispersion of Pt on Mg(Al)O@Al₂O₃. The final Pt loading was determined by inductively coupled plasma optical emission spectrometer (ICP-OES) technique as being 0.08 wt%, 0.13 wt%, 0.70 wt%, or 1.67 wt% on Mg(Al)O@Al₂O₃, affording 0.08 %, 0.13 %, 0.70 %, or 1.67 % Pt/Mg(Al)O@Al₂O₃-IR (IR represents in situ reduction). The Pt dispersion, calculated on the basis of hydrogen-oxygen titration (HOT) results, is 92 %, 84 %, 76 %, or 67 % for 0.08 %, 0.13 %, 0.70 %, or 1.67 % Pt/Mg(Al)O@Al₂O₃-IR (Table S1). For all Pt-containing sample, the specific surface areas are similar, in the range of 116-133 m² g⁻¹ (Table S1).

1
2
3 For 0.08 % Pt/Mg(Al)O@Al₂O₃-IR, Pt clusters and a few isolated Pt atoms are observed in
4 the HAADF-STEM image (Figure 1a). Increasing the Pt-loading to 0.13 %, 0.70 %, and 1.67 %,
5
6 Pt clusters get more dominant, showing gradually increased density of clusters with average sizes
7
8 of 0.9, 1.2, and 1.6 nm (Figure 1b-d). Very few single atoms or > 2.0 nm particles could be
9
10 observed for 0.13 %, 0.70 %, or 1.67 % Pt/Mg(Al)O@Al₂O₃-IR (Figure 1b-d). According to the
11
12 brightness intensity profile analysis (Figure S4), two types of Pt clusters in Pt/Mg(Al)O@Al₂O₃-
13
14 IR could be classified: (1) two-dimensional (2D) clusters composed of loose ensembles with
15
16 one-atom-thick and (2) three-dimensional (3D) clusters with multi-atom-thick in a size at
17
18 maximum distribution of 0.8-2.0 nm. The Pt dispersion, calculated on the basis of hydrogen-
19
20 oxygen titration (HOT) results, is 92 % for 0.08 % Pt/Mg(Al)O@Al₂O₃-IR, and decreases
21
22 gradually with increasing Pt loading (Table S1). To obtain atomically dispersed Pt in 100
23
24 percentage, 0.08 % Pt/Mg(Al)O@Al₂O₃-OR (OR represents oxidation in air followed by
25
26 reduction in H₂) was produced by first calcination of 0.10 % Pt²⁺/MgAl-LDHs@Al₂O₃ in air at
27
28 400 °C, and then holding in H₂ at 300 °C, affording a Pt dispersion of up to 98 % (Table S1). In
29
30 the HAADF-STEM image, Pt is observed exclusively as atomic dispersion for 0.08 %
31
32 Pt/Mg(Al)O@Al₂O₃-OR (Figure 1e). Similar procedure has been used to produce supported
33
34 atomic Pt in a previous report.⁴⁰ To estimate the distribution of engineered Pt species, at least
35
36 300 of atomic Pt, 2D Pt clusters, and 3D Pt clusters in more than four regions are randomly
37
38 selected. The statistic distribution of Pt species for 0.08 %, 0.13 %, 0.70 %, and 1.67 %
39
40 Pt/Mg(Al)O@Al₂O₃-IR and 0.08 % Pt/Mg(Al)O@Al₂O₃-OR is calculated and illustrated in
41
42 Figure 1f. For Pt/Mg(Al)O@Al₂O₃-IR, Pt sites changes from atom-thick dispersion (2D cluster)
43
44 coexisting with 3D clusters gradually to 3D clusters with Pt loading increasing from 0.08 to 1.67
45
46
47
48
49
50
51
52
53
54
55
56
57
58
59
60

1
2
3 % . The percentage of 2D/3D Pt clusters has been estimated as being 36/53, 23/69, 13/80, and
4
5 3/95 for 0.08 %, 0.13 %, 0.70 %, and 1.67 % Pt/Mg(Al)O@Al₂O₃-IR.
6
7

8
9 Pt coordination was characterized by extended X-ray absorption fine structure (EXAFS)
10 spectra (Figure 1g). The parameters of Pt-containing samples based on the EXAFS analysis are
11 shown in Table 1. The detailed fitting results of R-space and K-space are presented in Figure S5
12 and Figure S6. For 0.08 % Pt/Mg(Al)O@Al₂O₃-IR, Pt-O contribution ($N_{\text{Pt-O}} = 2.0$) is observed
13 much predominant over Pt-Pt contribution ($N_{\text{Pt-Pt}} = 3.7$) from the EXAFS spectrum. The Pt-Pt
14 contribution is hardly resolved despite the co-existence of 3D Pt clusters with atomic Pt and
15 atom-thick Pt clusters. The Pt-Pt coordination number for 0.08 % Pt/Mg(Al)O@Al₂O₃-IR is
16 much lower than for bulk Pt (coordination number of 12) as well. The results indicate that the 3D
17 clustered Pt sites here are highly coordination-unsaturated, even close to Pt-Pt coordination in
18 atom-thick dispersion, which is highly consistent with a Pt dispersion of 92 %. Pt-Pt contribution
19 becomes more visible (Figure 1g) and Pt-Pt coordination number (Table 1) increases with
20 increasing Pt loading. Pt-Pt contribution predominates over Pt-O contribution for 1.67 %
21 Pt/Mg(Al)O@Al₂O₃-IR, with a Pt-Pt coordination number of 6.2, corresponding to the
22 coordination-unsaturated atoms at corners/edges⁴¹ of Pt particles ($N_{\text{Pt-Pt}} = 4-7$). Atomically
23 dispersed Pt (0.08 % Pt/Mg(Al)O@Al₂O₃-OR) possesses a Pt-O coordination of 3.7 and no Pt-Pt
24 coordination, indicative of the strong interaction between atomic Pt and Mg(Al)O (Table 1). By
25 combining HAADF-STEM and XAFS techniques, atomic Pt, coordination-unsaturated Pt-Pt in
26 atom-thick dispersion (2D clusters), and coordination-unsaturated 3D Pt-Pt (3D clusters) have
27 been identified.
28
29
30
31
32
33
34
35
36
37
38
39
40
41
42
43
44
45
46
47
48
49
50
51
52

53 In the X-ray absorption near-edge structure (XANES) spectra (Figure 1h), each
54 Mg(Al)O@Al₂O₃ supported Pt displays a white line intensity between PtO₂ and Pt foil,
55
56
57
58
59
60

indicative of electron transfer due to Pt-O contribution and high dispersion of Pt. The white line intensity of supported Pt (Table S2) decreases in the sequence of single atoms > 2D clusters > 3D clusters (0.08 % Pt/Mg(Al)O@Al₂O₃-OR > 0.08 % > 0.13 % \approx 0.70 % > 1.67 % Pt/Mg(Al)O@Al₂O₃-IR). The white line results from the electron transition from 2p orbitals to 5d orbitals. A higher intensity of white line indicates larger amount of unoccupied 5d orbitals of Pt, and thus more positively charged Pt. The atomic Pt in 0.08 % Pt/Mg(Al)O@Al₂O₃-OR shows a white line intensity adjacent to PtO₂, suggesting that the atomic Pt is partially positively-charged. 0.08 % Pt/Mg(Al)O@Al₂O₃-IR shows stronger white line intensity than 0.13, 0.70, and 1.67 % Pt/Mg(Al)O@Al₂O₃-IR, suggesting more electron transfer from the Pt-Pt in atom-thick dispersion to support than from coordination-unsaturated 3D Pt-Pt. The Pt-Pt sites in atom-thick dispersion are electron-deficient in comparison to coordination-unsaturated 3D Pt sites. The 3D Pt clusters (1.67 % Pt/Mg(Al)O@Al₂O₃-IR) show a white line intensity adjacent to Pt foil.

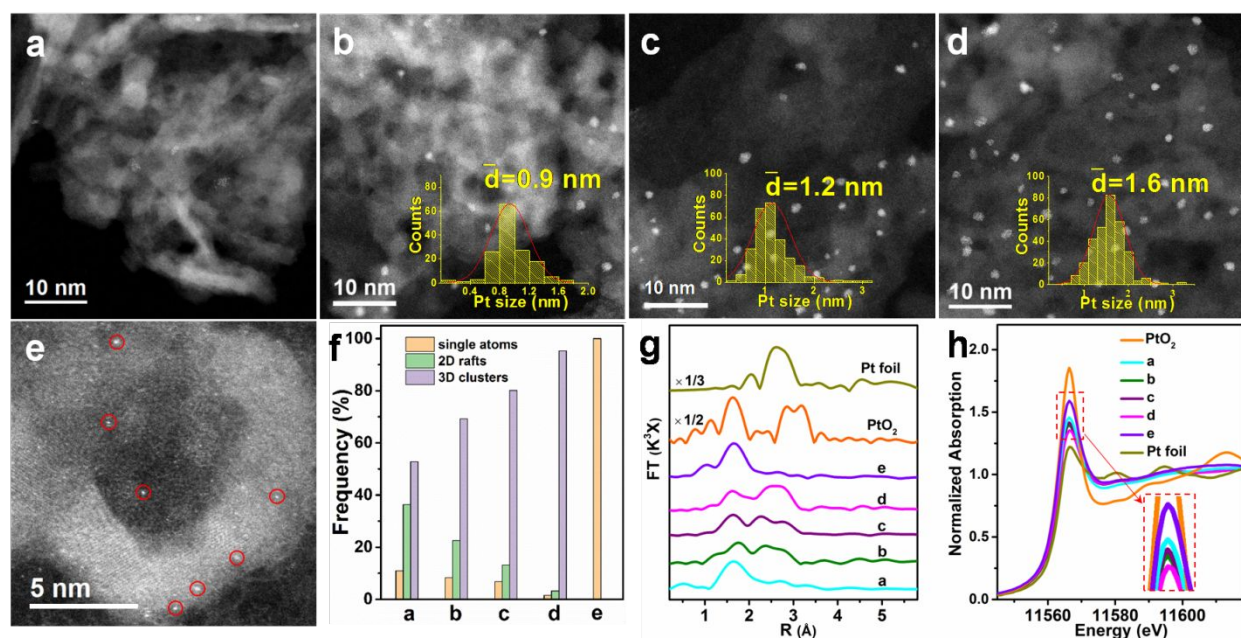


Figure 1. HAADF-STEM images of (a) 0.08 % Pt/Mg(Al)O@Al₂O₃-IR, (b) 0.13 % Pt/Mg(Al)O@Al₂O₃-IR, (c) 0.70 % Pt/Mg(Al)O@Al₂O₃-IR, (d) 1.67 % Pt/MgAlO@Al₂O₃-IR,

and (e) 0.08 % Pt/Mg(Al)O@Al₂O₃-OR; the inserts for b-d are the size distribution of Pt. (f) Distribution statistics of Pt dispersion based on brightness intensity results. (g) Fourier-transform EXAFS spectra and (h) normalized XANES spectra at Pt L_{III}-edge.

Table 1. EXAFS fitting parameters at the Pt L_{III}-edge for various samples

Sample	Shell	N^a	R (Å) ^b	σ^2 (Å ² ·10 ⁻³) ^c	ΔE_0 (eV) ^d	R factor (%)
0.08 % Pt/Mg(Al)O@Al ₂ O ₃ -IR	Pt-O	2.0	2.02	2.9	11.7	1.0
	Pt-Pt	3.7	2.67	12.0	4.2	
0.13 % Pt/Mg(Al)O@Al ₂ O ₃ -IR	Pt-O	1.8	2.02	7.6	9.7	1.9
	Pt-Pt	4.8	2.73	12.1	8.3	
0.70 % Pt/Mg(Al)O@Al ₂ O ₃ -IR	Pt-O	1.6	2.02	5.8	10.1	2.8
	Pt-Pt	5.1	2.73	8.6	8.0	
1.67 % Pt/Mg(Al)O@Al ₂ O ₃ -IR	Pt-O	1.0	1.99	2.5	5.5	1.0
	Pt-Pt	6.2	2.70	12.0	5.1	
0.08 % Pt/Mg(Al)O@Al ₂ O ₃ -OR	Pt-O	3.7	2.03	7.7	13.75	0.8
	Pt-Pt	6.2	2.70	12.0	5.1	
1.67 % Pt/Mg(Al)O@Al ₂ O ₃ -NR	Pt-O	0.6	1.94	2.0	-4.0	1.0
	Pt-Pt	7.3	2.74	6.7	7.0	
Pt foil	Pt-Pt	12	2.76	3.7	6.1	0.3
PtO ₂	Pt-O	6	2.01	4.1	7.2	0.7
	Pt-Pt	6	3.09	9.8	2.1	

^a N : coordination numbers; ^b R : bond distance; ^c σ^2 : Debye–Waller factor value, where the high σ^2 suggests a high degree of disorder of Pt; ^d ΔE_0 : inner potential correction to account for the difference in inner potential between the sample and the reference compound. R factor: goodness of fit; better is the curve fitted, smaller is the R-factor value got; generally, an acceptable R-

1
2
3 factor should be smaller than 5 %. S_0^2 were respectively set as 0.858/0.9 for Pt-Pt/Pt-O, which
4 were obtained from the experimental EXAFS fit of Pt foil/PtO₂ reference by fixing CN as the
5 known crystallographic value and was fixed to all the samples. Error bounds (accuracies) of the
6 above structural parameters were estimated as N , ± 20 %; R , ± 1 %; σ^2 , ± 20 %; ΔE_0 , ± 20 %.

15
16 Pt/Mg(Al)O@Al₂O₃ was then used as catalyst for the hydroconversion of furfuryl alcohol in
17 a continuous-flow system using a fixed-bed reactor at 200 °C with a WHSV of 0.12 h⁻¹. The
18 qualitative identifications of each product are based on the results from ¹H and ¹³C nuclear
19 magnetic resonance (NMR) spectra and mass spectra (MS) (see details in the Supporting
20 Information, Appendix). No visible change in the furfuryl alcohol conversion or product
21 selectivity is observed in a 6-h online reaction for each sample (Figure S7). Thus initial
22 conversion and selectivity are selected for discussion (Table 2). Atomic Pt (0.08 %
23 Pt/Mg(Al)O@Al₂O₃-OR) affords a selectivity of 93 % to 2-methylfuran (2-MF), with a furfuryl
24 alcohol conversion of 87 %. That means the hydrogenolysis of C-OH is preferred on atomic Pt,
25 affording 2-MF. On coordination-unsaturated Pt-Pt in atom-thick dispersion coexisting with
26 highly coordination-unsaturated 3D Pt (0.08 % Pt/Mg(Al)O@Al₂O₃-IR), both of
27 tetrahydrofurfuryl alcohol (THFA) and 1,2-pentanediol (1,2-PeD) have been observed as the
28 main products, with a selectivity of 43 % to 1,2-PeD and 34 % to THFA under 41 % conversion
29 of furfuryl alcohol. 1,5-pentanediol (1,5-PeD) is detected as major by-product. With
30 coordination-unsaturated 3D Pt sites gradually predominating (0.13, 0.70 to 1.67 %
31 Pt/Mg(Al)O@Al₂O₃-IR), the selectivity to 1,2-PeD increases, and the selectivity to either THFA
32 or 1,5-PeD decreases. The conversion of furfuryl alcohol also increases with increasing content
33 of 3D Pt clusters. A selectivity of up to 86 % to 1,2-PeD has been achieved with complete

conversion of furfuryl alcohol on the Pt sites almost completely present in 3D clusters (1.67 % Pt/Mg(Al)O@Al₂O₃-IR). According to previous reports, H-transfer hydrogenation of furfural-to-furfuryl alcohol, furfural-to-2-methylfuran or ethanol-to-n-butanol is efficient using alcohol as hydrogen donor, for liquid-solid phase reaction in the autoclave⁴²⁻⁴⁴ or gas-solid phase reaction under N₂^{45,46}. To better understand the role of Pt in this work, Mg(Al)O@Al₂O₃ (without Pt) has been produced by the thermal treatment of MgAl-LDHs@Al₂O₃ in H₂ at 400 °C. The hydro-conversion of furfuryl alcohol on Mg(Al)O@Al₂O₃ has been tested, showing barely conversion of furfuryl alcohol and no product (Table 2). The result indicates the effect of H-transfer hydrogenation with ethanol as hydrogen carrier could be ignored in our system.

Table 2. Hydrogenation of furfuryl alcohol at 200 °C over each sample

Sample	Con. (%)	Sel. (%)				
		THFA	2-MF	1,5-PeD	1,2-PeD	Others
0.08 % Pt/Mg(Al)O@Al ₂ O ₃ -OR	87 (88)	6 (7)	93 (92)	0 (0)	0 (0)	1 (1)
0.08 % Pt/Mg(Al)O@Al ₂ O ₃ -IR	41	34	8	15	41	2
0.13 % Pt/Mg(Al)O@Al ₂ O ₃ -IR	65	15	2	13	64	6
0.70 % Pt/Mg(Al)O@Al ₂ O ₃ -IR	98	7	1	7	80	5
1.67 % Pt/Mg(Al)O@Al ₂ O ₃ -IR	> 99	6	1	5	86	2
0.08 % Pt/Mg(Al)O@Al ₂ O ₃ -OR-R	41	24	4	12	56	4
1.67 % Pt/Mg(Al)O@Al ₂ O ₃ -NR	> 99	14	3	8	73	2
0.70 % Pt/Al ₂ O ₃ -IR	96	15	16	3	62	4
Mg(Al)O@Al ₂ O ₃	< 1	-	-	-	-	-

Reaction conditions: 0.2 mol/L furfuryl alcohol (ethanol as solvent), 1 g of catalysts, WHSV = 0.12 h⁻¹, 200 °C, 3 MPa H₂. Pentanol and HPO was included in others. The data in parentheses are the reproduced experimental data.

1
2
3 To allow selectivity comparison, the conversion is controlled at the same level (~ 20 %) by
4 changing the contact time or under a mild condition (160 °C) (Table 3). The calculated turnover
5 frequency (TOF) for atomic Pt (0.08 % Pt/Mg(Al)O@Al₂O₃-OR) is 45 h⁻¹ (Table 3, entry 1),
6 with a selectivity of 17 % and 35 % to THFA and 1,2-PeD under 160 °C. Lower selectivity to 2-
7 MF under 160 °C than under 200 °C indicates that higher temperature is beneficial to the
8 selective activation of C-OH in furfuryl alcohol on atomic Pt. On Pt-Pt site, the TOF value
9 gradually decreases with increasing content of 3D Pt clusters (Table 3, entry 2-5), from 66 h⁻¹ for
10 0.08 % Pt/Mg(Al)O@Al₂O₃-IR with 36 % of 2D cluster and 53 % of 3D cluster to 48 h⁻¹ for 1.67
11 % Pt/Mg(Al)O@Al₂O₃-IR with 91 % of 3D cluster, indicative of the higher activity of
12 coordination-unsaturated Pt-Pt in atom-thick dispersion than coordination-unsaturated 3D Pt-Pt.
13 On 0.13 % Pt/Mg(Al)O@Al₂O₃-IR, 1-hydroxypenta-2-one (HPO) was detected in a selectivity of
14 28 % under 160 °C and a WHSV of 0.19 h⁻¹ while in 7 % (Table 3, entry 6) under a longer
15 contact time (WHSV of 0.12 h⁻¹). Under a much shorter contact time (WHSV of 0.36 or 1.44 h⁻¹),
16 HPO was also detected on 0.70 % Pt/Mg(Al)O@Al₂O₃-IR or 1.67 % Pt/Mg(Al)O@Al₂O₃-IR
17 (Table 3, entry 7 or 8). But the selectivity to total HPO and 1,2-PeD hardly changes with contact
18 time at 160 °C, and is also similar to the selectivity to 1,2-PeD at 200 °C, indicating HPO might
19 serve as an important intermediate for the formation of 1,2-PeD. By prolonging the contact time
20 at 160 °C, HPO is converted to 1,2-PeD. In a previous report,⁴⁷ 1,2-PeD or 1,5-PeD was
21 produced from THFA with high H₂ pressure. Employing THFA as the substrate here (Table S3),
22 THFA is hardly transformed with no product detected over 1.67 % Pt/Mg(Al)O@Al₂O₃-IR. The
23 results indicate that THFA is not a necessary intermediate for the production of pentanediols
24 from furfuryl alcohol in this work. Employing furfural as the substrate (Table S3), 1,2-PeD is
25 also produced in a yield of 78 %. The conversion of furfuryl alcohol to 1,2-PeD (a selectivity of
26
27
28
29
30
31
32
33
34
35
36
37
38
39
40
41
42
43
44
45
46
47
48
49
50
51
52
53
54
55
56
57
58
59
60

86 %) or PeDs (a selectivity of 91 %) on coordination-unsaturated 3D Pt sites in this work is superior to those of the state-of-the-art catalysts.

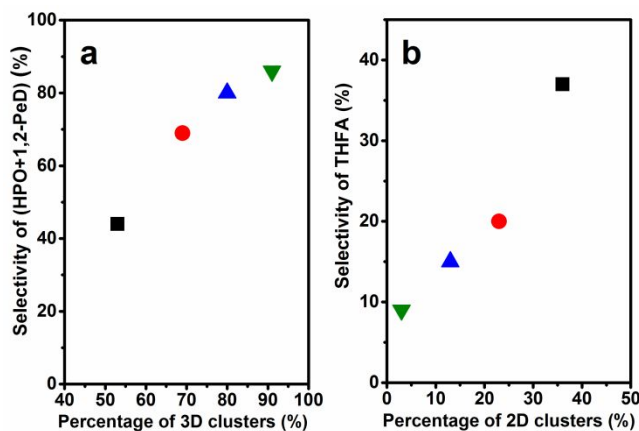
Table 3. Hydrogenation of furfuryl alcohol at 160 °C over each Pt sample

Entry	Sample	Con. (%)	Sel. (%)							TOF (h ⁻¹)
			THFA	2-MF	1,5-PeD	HPO	1,2-PeD	1,2-PeD + HPO	Others	
1	0.08 % Pt/Mg(Al)O @Al ₂ O ₃ -OR	15 (17)	17 (17)	41 (43)	5 (5)	1 (1)	35 (35)	36 (36)	1 (1)	45
2	0.08 % Pt/Mg(Al)O @Al ₂ O ₃ -IR	21	37	4	14	1	43	44	1	66
3	0.13 % Pt/Mg(Al)O @Al ₂ O ₃ -IR [§]	18	20	1	9	28	41	69	1	60
4	0.70 % Pt/Mg(Al)O @Al ₂ O ₃ -IR [#]	21	15	1	5	30	50	80	1	51
5	1.67 % Pt/Mg(Al)O @Al ₂ O ₃ -IR [*]	19	9	1	4	17	68	85	1	48
6	0.13 % Pt/Mg(Al)O @Al ₂ O ₃ -IR	30	16	1	10	7	64	71	2	
7	0.70 % Pt/Mg(Al)O @Al ₂ O ₃ -IR	52	11	1	5	12	70	82	1	
8	1.67 % Pt/Mg(Al)O @Al ₂ O ₃ -IR	96 (95)	6 (5)	1 (1)	6 (6)	1 (1)	85 (85)	86 (86)	2 (2)	

Reaction conditions: 0.2 mol/L furfuryl alcohol (ethanol as solvent), 1 g of catalysts, WHSV = 0.12 h⁻¹, [§]WHSV = 0.19 h⁻¹, [#]WHSV = 0.36 h⁻¹, ^{*}WHSV = 1.44 h⁻¹, 160 °C, 3 MPa of H₂. Pentanol was included in others. The data in parentheses are the reproduced experimental data.

Relating the product selectivity with the Pt dispersion on Mg(Al)O under similar conversion of furfuryl alcohol, it can be found that the selectivity of (HPO + 1,2-PeD) increases with the increase in the percentage of coordination-unsaturated 3D Pt (3D cluster) (Figure 2a), while the selectivity of THFA resulting from the hydrogenation of ring C=C increases (Figure 2b) with increasing percentage of coordination unsaturated Pt-Pt sites in atom-thick dispersion (2D

1
2
3 cluster). The results for the hydroconversion of furfuryl alcohol on 0.08 % Pt/Mg(Al)O@Al₂O₃-
4
5 OR unambiguously prove that 2-MF are generated by the hydrogenolysis of C-OH on atomic Pt.
6
7 Interestingly, the selectivities to total of 1,2-PeD and HPO are similar under varied conversions
8
9 over each clustered Pt sample (Pt/Mg(Al)O@Al₂O₃-IR) in this work, indicative of the
10
11 enhancement of activity without sacrificing selectivity. In heterogeneous catalysis, achieving
12
13 supported metal with simultaneously enhanced activity and stability is of vital importance and
14
15 remains a challenging goal. The achievement in this work is probably attributed to the dilute
16
17 solution of furfuryl alcohol in ethanol, which leads to the insensitive of selectivity to reactant
18
19 concentration. The role of solvent and reactant concentration on selectivity deserves an in-depth
20
21 investigation, which is scheduled in our subsequent research.
22
23
24
25
26
27
28
29
30



31
32
33
34
35
36
37
38
39
40
41
42
43
44
45 **Figure 2.** Variation of (a) the selectivity of (HPO + 1,2-PeD) with the percentage of 3D clusters
46 and (b) THFA selectivity with the percentage of 2D clusters over 0.08 % Pt/Mg(Al)O@Al₂O₃-IR
47 (black square), 0.13 % Pt/Mg(Al)O@Al₂O₃-IR (red circle), 0.70 % Pt/Mg(Al)O@Al₂O₃-IR (blue
48 triangle), and 1.67 % Pt/Mg(Al)O@Al₂O₃-IR (green inverted triangle).
49
50
51
52
53
54
55
56
57
58
59
60

To further confirm the sensitivity of the selective activation of furan C-O-C, branched C-OH, or ring C=C to the nature of Pt sites, the as-prepared 0.08 % Pt/Mg(Al)O@Al₂O₃-OR was re-treated by calcination in H₂ at 400 °C (denoted 0.08 % Pt/Mg(Al)O@Al₂O₃-OR-R) to convert Pt dispersion from single atoms to clusters. Pt clusters are clearly observed for 0.08 % Pt/Mg(Al)O@Al₂O₃-OR-R in the HAADF-STEM image (Figure 3a), with 32 % of 2D cluster and 59 % of 3D cluster according to the brightness intensity profile analysis. Based on the 2D/3D percentage, the Pt dispersion for 0.08 % Pt/Mg(Al)O@Al₂O₃-OR-R is similar to that for 0.08 % Pt/Mg(Al)O@Al₂O₃-IR. In the hydrogenation of furfuryl alcohol at 200 °C (Table 2), the major product has been changed from 2-MF (93 % of selectivity) on atomic Pt to 1,2-PeD and THFA in the selectivity of 56 % and 24 % on 3D and 2D Pt clusters. Just as expected, the activation of chemical bonds in furfuryl alcohol highly depends on the dispersion of Pt sites. On the other hand, Pt particles with higher Pt-Pt coordination number (Table 1) have been prepared by first thermal treatment of 1.80 % Pt²⁺/MgAl-LDHs@Al₂O₃ in N₂ at 400 °C and then reduction in H₂ at 400 °C (denoted 1.67 % Pt/Mg(Al)O@Al₂O₃-NR, NR represents thermal treatment in N₂ followed by reduction in H₂). In the XRD pattern (Figure S3f), the reflection of Pt (111) at 40.1 ° is observed for 1.67 % Pt/Mg(Al)O@Al₂O₃-NR, indicative of the existence of Pt nanoparticles. Based on TEM/HR-TEM images, the average size of Pt particles is 3.5 nm (Figure 3b), with exposure of 100 and 111 planes of cub-octahedrons (Figure 3c). Comparing Pt particles (1.67 % Pt/Mg(Al)O@Al₂O₃-NR) with coordination-unsaturation 3D clusters (1.67 % Pt/Mg(Al)O@Al₂O₃-IR) in the hydrogenation of furfuryl alcohol (Table 2), the selectivity to 1,2-PeD decrease from 86 % to 73 % with Pt dispersion changing from coordination-unsaturation 3D clusters to nanoparticles, while the selectivity to THFA increases from 6 % to 14 %. The results indicate that the formation of 1,2-PeD requires coordination-unsaturated 3D Pt-Pt like at

corners/edges, rather than terrace Pt-Pt. Our observation with Pt particles (1.67 % Pt/Mg(Al)O@Al₂O₃-NR) is consistent with previous report³⁰ that the hydrogenation of C=C bonds in furfural is favored on terrace (such as 111 plane) metal sites. Based on the above results, the reaction pathways for the hydrogenation of furfuryl alcohol over varied Pt sites on Mg(Al)O are proposed as Figure 4, which are to be further discussed and proved in the next context.

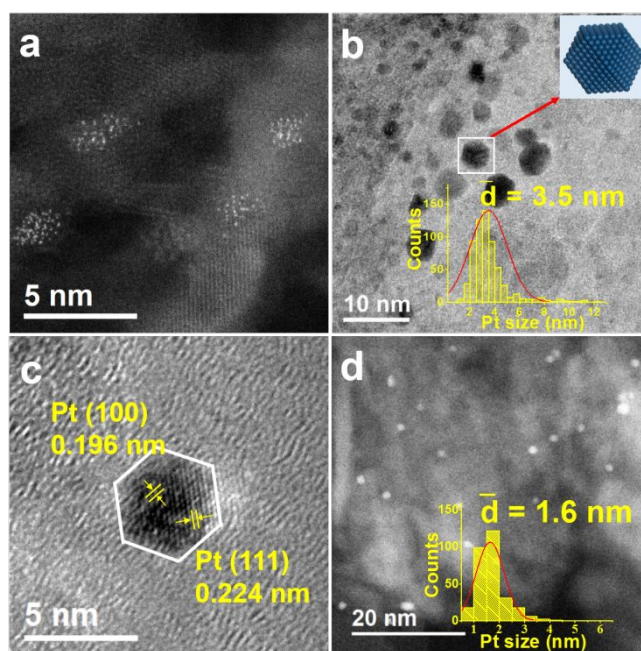


Figure 3. HAADF-STEM or TEM images of (a) 0.08 % Pt/Mg(Al)O@Al₂O₃-OR-R, (b and c) 1.67 % Pt/Mg(Al)O@Al₂O₃-NR, and (d) 0.72 % Pt/Al₂O₃-IR.

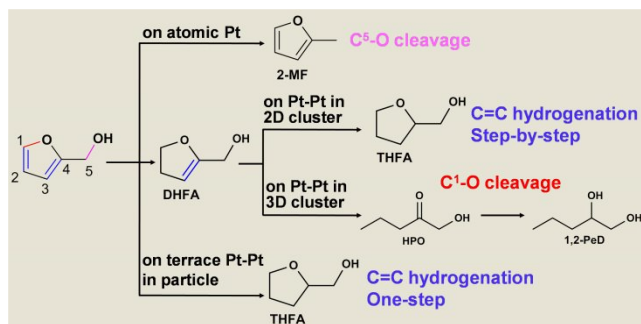


Figure 4. Proposed reaction paths for the hydrogenation of furfuryl alcohol over engineered Pt sites.

1
2
3 To clarify the Pt-dispersion dependent hydrogenation of furfuryl alcohol, the FT-IR spectra
4 recorded surface reaction experiments are performed (Figure 5 and 6). On atomic Pt (0.08 %
5 Pt/Mg(Al)O@Al₂O₃-OR), the absorption bands assigned^{48,49} to C¹-O at 1076 cm⁻¹, C⁵-O linearly
6 adsorbed with O terminal at 1102 cm⁻¹, C¹-O-C⁴ at 1149 cm⁻¹, C²-C³ at 1221 cm⁻¹, C¹=C² at
7 1504 cm⁻¹, and C³=C⁴ at 1596 cm⁻¹ in furfuryl alcohol are observed (Figure 5; see assignments
8 of the absorption bands in the Supporting Information, Appendix). With on-stream time under
9 hydrogenation conditions, the absorption intensity of C³=C⁴ at 1596 cm⁻¹ gradually increases
10 relative to that of C¹=C² at 1504 cm⁻¹ with the vanishment of O-terminal adsorption at 1102
11 cm⁻¹, and new bands assigned to methyl emerge at 2877 and 2961 cm⁻¹ and become more visible
12 with time. Other change of furan-ring are hardly observed. According to previous observation,⁴⁸
13 the IR absorption of C³=C⁴ in 2-MF is visible while very weak in furfuryl alcohol. So the gradual
14 increase in the absorption intensity of C³=C⁴ originates from the conversion of furfuryl alcohol to
15 2-MF. As discussed above, the atomic Pt sites are electron-deficient. The electron-deficient
16 atomic Pt sites prefer an O-terminal adsorption, leading to the targeted activation of C⁵-O (Figure
17 5). The targeted activation of C⁵-O with O-terminal adsorption on atomic Pt^{δ+} sites accounts for
18 the C⁵-O cleavage without affecting the furan C-O and ring C=C, affording 2-MF as major
19 product as illustrated in Figure 4.
20
21
22
23
24
25
26
27
28
29
30
31
32
33
34
35
36
37
38
39
40
41
42
43
44
45
46
47
48
49
50
51
52
53
54
55
56
57
58
59
60

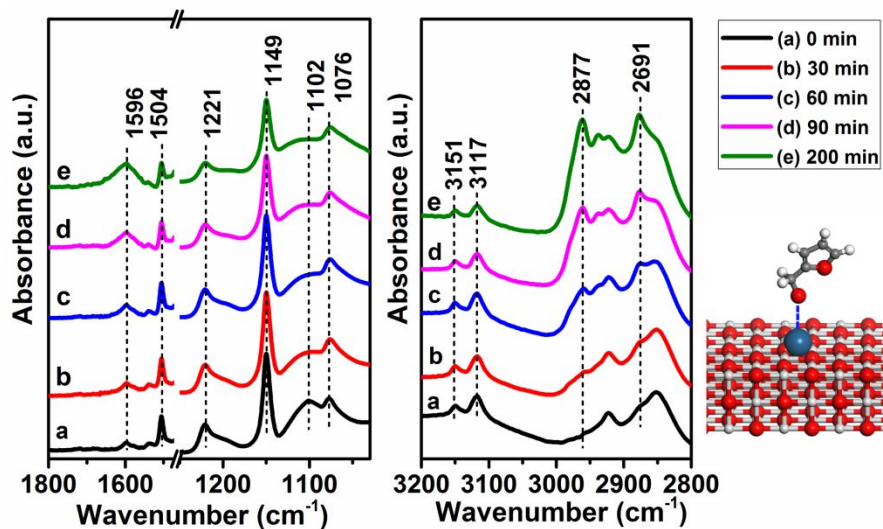


Figure 5. FT-IR spectra recorded hydrogenation progress of furfuryl alcohol at 80 °C at intervals in H₂/Ar flow on 0.08 % Pt/Mg(Al)O@Al₂O₃-OR; the insert is the proposed adsorption model.

On coordination-unsaturated 3D Pt-Pt sites (3D clusters in 1.67 % Pt/Mg(Al)O@Al₂O₃-IR), the hydrogenation of furfuryl alcohol occurs much more rapidly than on atomic Pt, with the transformation of chemical bonds almost finished in 10 min. The absorption of furan C¹-O-C⁴ at 1149 cm⁻¹, ring C²-C³ and C¹=C² at 1221 and 1504 cm⁻¹ in furfuryl alcohol gradually decrease in intensity with on-stream time and eventually disappears in 10 min under hydrogenation conditions (Figure 6A), indicative of the hydrogenation of ring C¹=C² and the hydrogenolysis of whole furan structure. Meanwhile, new bands at 1064 and 1694 cm⁻¹ are observed to emerge since 1 min and gradually increase in intensity, and a band at 1128 cm⁻¹ emerges at 10 min. The bands at 1064 and 1128 cm⁻¹ well agree with the C-O vibrations in 1,2-PeD,⁴⁸ indicating the formation of 1,2-PeD. The band at 1694 cm⁻¹, assigned⁴² to C=O in O-terminal adsorption, originates from HPO here, as observed in the catalytic results (Table 3) as key intermediate of 1,2-PeD. The adsorbed C=O bond likely results from the transformation from C³=C⁴-OH, formed by the cleavage of C¹-O, to C³-C⁴=O. On the basis of the observation above, the

1
2
3 conversion of furfuryl alcohol to 1,2-PeD can be proposed to start from the hydrogenolysis of
4 furan structure. Unfortunately, it is hard to clearly distinguish step-by-step hydrogenolysis and
5 one-step hydrogenolysis for now because no specific intermediates have been detected in the -
6
7 FT-IR spectra. But from the incomplete vanishment of C¹-O at 1076 cm⁻¹ and C³=C⁴ at 1596
8 cm⁻¹, 1,2-dihydrofurfuryl alcohol (1,2-DHFA) can be deduced as an intermediate. It has also
9
10 been reported⁹ that C¹=C² bond of furfuryl alcohol can be hydrogenated to form 1,2-DHFA. In
11 1,2-DHFA, C¹-O linkage, located adjacent to the just-formed C¹-C² linkage, is easier to get
12 adsorbed on coordination-unsaturated 3D Pt-Pt sites. Furthermore, C¹-O is weakened due to the
13 p- π conjugation of O-C⁴=C³ linkage, facilitating the cleavage of C¹-O to result in ring-opening.
14
15 The ring-opened species from the cleavage of C¹-O is quickly converted to HPO, and 1,2-PeD is
16 produced from the hydrogenation of C=O of HPO, as illustrated in Figure 4.
17
18
19
20
21
22
23
24
25
26
27
28

29
30 On 2D cluster coexisting with highly coordination-unsaturated 3D cluster (0.08 %
31 Pt/Mg(Al)O@Al₂O₃-IR), the emergence of C=O of HPO at 1694 cm⁻¹ and C-O vibration in 1,2-
32 PeD at 1128 cm⁻¹ indicate the formation of 1,2-PeD owing to the hydrogenolysis of furan ring
33 via HPO (Figure 6B), just as observed on coordination-unsaturated 3D Pt-Pt. The absorption of
34 C³=C⁴ at 1596 cm⁻¹ becomes intensive with on-stream time in the case of no 2-MF formation
35 and C¹=C² at 1504 cm⁻¹ becomes weaker till to disappearance, indicating the formation of semi-
36 hydrogenation product. So the THFA observed in the catalytic results (Table 3) can be proposed
37 to produce by step-by-step hydrogenation via 1,2-DHFA as the intermediate, as illustrated in
38 Figure 4. The incompletely vanished C¹-O-C⁴ at 1149 cm⁻¹ and the gradually intensified C¹-O at
39 1074 cm⁻¹ indicate the preservation of furanic ring structure. In the FT-IR spectrum of THFA,
40 the band around 1074 cm⁻¹ is the only absorption in the range of 1000~1200 cm⁻¹,⁴⁸ consistent
41 with our conclusion. THFA has also been observed on supported Pt particles (1.67 %
42
43
44
45
46
47
48
49
50
51
52
53
54
55
56
57
58
59
60

Pt/Mg(Al)O@Al₂O₃-NR). But it can be seen from the FT-IR spectra recorded surface reaction (Figure S8) that the intensity of C¹=C² at 1504 cm⁻¹ and C³=C⁴ at 1596 cm⁻¹ simultaneously decrease in the hydrogenation, indicative of one-step hydrogenation of furfuryl alcohol to THFA.

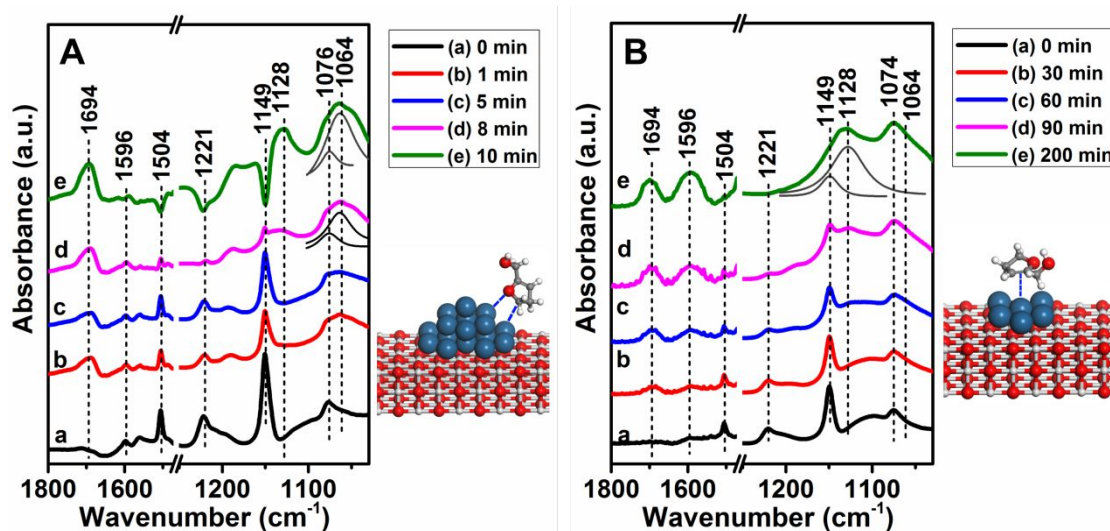


Figure 6. FT-IR spectra recorded hydrogenation progress of furfuryl alcohol at 80 °C at intervals in H₂/Ar flow on (A) 1.67 % Pt/Mg(Al)O@Al₂O₃-IR and (B) 0.08 % Pt/Mg(Al)O@Al₂O₃-IR; the inserts are the proposed adsorption models.

To further testify the reaction mechanism, FT-IR spectra recorded surface reaction on 3D Pt clusters (1.67 % Pt/Mg(Al)O@Al₂O₃-IR) is broken off by stopping H₂/Ar flow. After reaction in H₂/Ar flow for 2 min, Ar flow is introduced (Figure 7). The absorption bands of furan C¹-O-C⁴ at 1149 cm⁻¹, C²-C³ and C¹=C² at 1221 and 1504 cm⁻¹ in furfuryl alcohol gradually decrease in intensity but incompletely vanish, and the absorption bands of C=O at 1694 cm⁻¹ and C-O at 1128 cm⁻¹ in HPO gradually increase in intensity under Ar flow, indicating the initially converted furfuryl alcohol could further be transformed to HPO. The results prove the observed bands in the FT-IR spectra represent the active species. However, the absorption band of HPO (C=O) continuously becomes enhanced under Ar flow, while no visible band for 1,2-PeD (C-O

at 1064 cm^{-1}) is observed, indicating the hydrogenation of C=O in HPO to produce 1,2-PeD is restrained with the lack of H_2 .

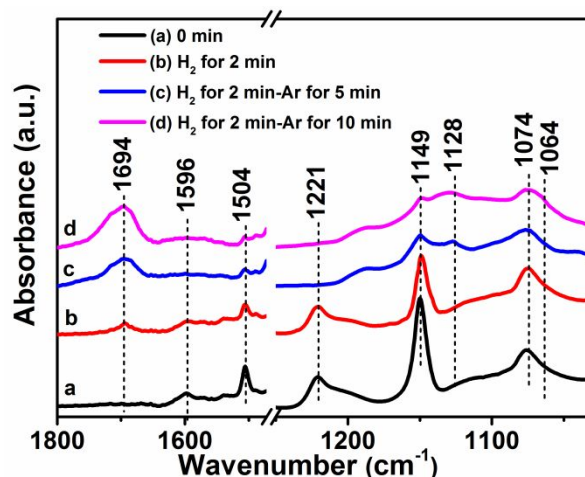


Figure 7. FT-IR spectra recorded hydrogenation progress of furfuryl alcohol at $80\text{ }^\circ\text{C}$ on 1.67 % Pt/Mg(Al)O@Al₂O₃-IR. After reaction in H_2/Ar flow for 2 min (a, b), Ar flow was introduced for 10 min (c, d) with the FT-IR spectra recorded at intervals.

As is well known, the surface property of the support could affect the catalytic performance. Therefore, in this work, the role of Mg(Al)O support toward hydrogenation of furfuryl alcohol has also been investigated. 0.72 % Pt/Al₂O₃-IR (without LDHs) has been prepared as a control by reduction of Pt²⁺-loaded Al₂O₃. 3D Pt clusters with average size of 1.6 nm, which is similar to that for 1.67 % Pt/Mg(Al)O@Al₂O₃-IR, are observed for 0.72 % Pt/Al₂O₃-IR (Figure 3d). The percentage of 2D/3D Pt clusters has been estimated as being 6/81 for 0.72 % Pt/Al₂O₃-IR. This indicates that on one hand Mg(Al)O promotes Pt dispersion more effectively than Al₂O₃. In the XANES spectra (Figure S9 and Table S2), 0.72 % Pt/Al₂O₃-IR displays the similar white line intensity as 1.67 % Pt/Mg(Al)O@Al₂O₃-IR. According to the CO₂-TPD profiles (Figure S10),

1
2
3 1.67 % Pt/Mg(Al)O@Al₂O₃-IR have stronger basicity and more basic sites than 0.72 %
4
5 Pt/Al₂O₃-IR. In the hydrogenation of furfuryl alcohol, 2-MF has been produced in a selectivity of
6
7 16 % over 0.72 % Pt/Al₂O₃-IR (Table 2), which is hardly observed over 1.67 %
8
9 Pt/Mg(Al)O@Al₂O₃-IR. In comparison to 1.67 % Pt/Mg(Al)O@Al₂O₃-IR, the selectivity to 1,2-
10
11 PeD decreases and the selectivity to THFA increases on 0.72 % Pt/Al₂O₃-IR. The selectivity to
12
13 1,2-PeD is positively related with the amount of basic sites in this work, which is consistent with
14
15 the observation in an earlier report.¹⁰ The basic site on Mg(Al)O is supposed to help abstracting
16
17 H⁺ from C-OH^{50,51}, affording electron-rich alkoxide species (C-O⁻). The electron-rich alkoxide
18
19 species on one hand reinforces C-O⁻ and on the other hand makes furan C-O-C more
20
21 approachable to coordination-unsaturated Pt sites through donating electron, thus inhibiting the
22
23 cleavage of C-O⁻ and enhancing the breakage of furan C-O-C. In the FT-IR spectra for the
24
25 hydrogenation of furfuryl alcohol over 0.72 % Pt/Al₂O₃-IR (Figure S11), with the decrease in
26
27 intensity and/or gradual vanishment of C¹=C² at 1504 cm⁻¹, C²-C³ at 1221 cm⁻¹, and C¹-O-C⁴ at
28
29 1149 cm⁻¹, the absorption originating from C=O of HPO at 1701 cm⁻¹ and C-O of 1,2-PeD at
30
31 1128, and 1064 cm⁻¹ emerge, indicating the hydrogenation of ring C¹=C² and hydrogenolysis of
32
33 furan C¹-O-C⁴, accounting for the production of 1,2-PeD via HPO intermediate as well. In the
34
35 meantime, the absorption originating from C³=C⁴ at 1596 cm⁻¹ gradually increasing in intensity,
36
37 and adsorbed C⁵-O at 1102 cm⁻¹ disappears since 2 min on-stream, consistent with the formation
38
39 of 2-MF through the cleavage of C⁵-O. The FT-IR spectra recorded surface reaction in this work
40
41 could partially support the realistic catalytic results. Operando investigations under realistic
42
43 condition could provide more powerful evidence, and the experiments as well as the equipments
44
45 are being designed in our laboratory.
46
47
48
49
50
51
52
53
54
55
56
57
58
59
60

To investigate the dispersion stability of Pt, the spent atomic Pt or 3D Pt cluster, which has undergone a 6-h furfuryl alcohol hydrogenation reaction, has been characterized using HAADF-STEM technique. No visible change in the dispersion of Pt isolated-atoms in 0.08 % Pt/Mg(Al)O@Al₂O₃-OR or 3D clusters in 1.67 % Pt/Mg(Al)O@Al₂O₃-IR is observed after 6-h reaction at 200 °C (Figure 8), as well as no aggregated ensemble in low magnification image (Figure 8). The results also indicate the engineered Pt sites really serve as active sites during the reaction.

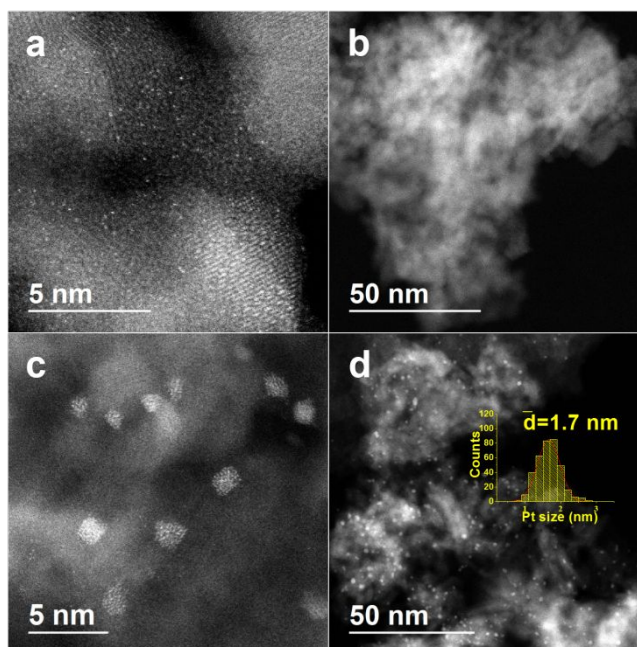


Figure 8. HAADF-STEM images with varied magnifications of spent (a, b) 0.08 % Pt/Mg(Al)O@Al₂O₃-OR and (c, d) 1.67 % Pt/MgAlO@Al₂O₃-IR after 6-h furfuryl alcohol hydrogenation reaction; the insert for (d) is the size distribution of Pt.

3. Conclusions

In summary, this work demonstrates an efficient selective activation to C-OH, C-O-C, or C=C on atomic Pt, coordination-unsaturated 2D Pt-Pt, or coordination-unsaturated 3D Pt-Pt in the hydroconversion of furfuryl alcohol, producing 2-MF, THFA or 1,2-PeD. The Pt sites are controlled by tailoring the Pt dispersion (single atom, 2D cluster, or 3D cluster) on Mg(Al)O support. The Pt-site dependent intrinsic reaction mechanisms have been traced with the FT-IR spectra recorded surface reaction. On atomic Pt, C-O-H is easily activated with O-terminal adsorption without affecting furan C-O and C=C. On coordination-unsaturated 2D Pt-Pt sites, the selective activation of C=C step-by-step to generate THFA takes place. On coordination-unsaturated 3D Pt-Pt sites, the hydrogenolysis of furan ring occurs through the cleavage of weakened and adsorbed furan C-O, affording 1,2-PeD as major product. The Mg(Al)O support also play a key role in promoting the selectivity to 1,2-PeD by providing basic sites. 1,5-PeD has also been detected on Pt clusters, but unfortunately in a low selectivity. The catalytically active sites for targeted activation of furan C-O to produce 1,5-PeD from furfural/furfuryl alcohol is worth deep exploring.

AUTHOR INFORMATION

Corresponding Author

* zhenglr@ihep.ac.cn (L. Zheng)

* hejing@mail.buct.edu.cn or jinghe@263.net.cn (J. He)

Notes

The authors declare no competing financial interest.

ASSOCIATED CONTENT

The Supporting Information is available free of charge via the Internet at <http://pubs.acs.org>.

Detailed experimental procedures, characterization and catalytic test methods; XRD patterns, SEM and STEM images, catalytic tests, EXAFS fitting curves, FT-IR spectra recorded surface reactions, and TPD profiles; appendix of ^1H and ^{13}C NMR spectra, mass spectrum, and assignments of the absorption bands in FT-IR spectra (PDF).

ACKNOWLEDGMENT

Financial supports from National Natural Science Foundation of China (21521005, 91634120), National Key R&D Program of China (2017YFA0206804), and the Fundamental Research Funds for the Central Universities (ZY1936 and XK1802-6) are gratefully acknowledged. The authors also thank the support from Beijing Engineering Center for Hierarchical Catalysts.

REFERENCES

- (1) Zakzeski, J.; Bruijninx, P. C. A.; Jongerius, A. L.; Weckhuysen, B. M. The Catalytic Valorization of Lignin for the Production of Renewable Chemicals. *Chem. Rev.* **2010**, *110*, 3552-3599.
- (2) Li, C.; Zhao, X.; Wang, A.; Huber, G. W.; Zhang, T. Catalytic Transformation of Lignin for the Production of Chemicals and Fuels. *Chem. Rev.* **2015**, *115*, 11559-11624.

1
2
3 (3) Zhang, Z.; Song, J.; Han, B., Catalytic Transformation of Lignocellulose into Chemicals
4 and Fuel Products in Ionic Liquids. *Chem. Rev.* **2017**, *117*, 6834-6880.

5
6
7
8 (4) Mika, L. T.; Csefalvay, E.; Nemeth, A. Catalytic Conversion of Carbohydrates to Initial
9 Platform Chemicals: Chemistry and Sustainability. *Chem. Rev.* **2018**, *118*, 505-613.

10
11
12
13 (5) Hoydonckx, H. E.; Van Rhijn, W. M.; Van Rhijn, W.; De Vos, D. E.; Jacobs, P. A.
14 *Furfural and Derivatives*. WileyVCH Verlag GmbH & Co. KGaA: Weinheim, **2012**.

15
16
17 (6) Li, X.; Jia, P.; Wang, T., Furfural: A Promising Platform Compound for Sustainable
18 Production of C₄ and C₅ Chemicals. *ACS Catal.* **2016**, *6*, 7621-7640.

19
20
21 (7) Mariscal, R.; Maireles-Torres, P.; Ojeda, M.; Sádaba, I.; López Granados, M. Furfural: A
22 Renewable and Versatile Platform Molecule for the Synthesis of Chemicals and Fuels. *Energy*
23 *Environ. Sci.* **2016**, *9*, 1144-1189.

24
25 (8) Yan, K.; Wu, G.; Lafleur, T.; Jarvis, C. Production, Properties and Catalytic Hydrogenation
26 of Furfural to Fuel Additives and Value-Added Chemicals. *Renewable Sustainable Energy Rev.*
27 **2014**, *38*, 663-676.

28
29 (9) Zhang, B.; Zhu, Y.; Ding, G.; Zheng, H.; Li, Y. Selective Conversion of Furfuryl Alcohol
30 to 1,2-Pentanediol over a Ru/MnO_x Catalyst in Aqueous Phase. *Green Chem.* **2012**, *14*, 3402-
31 3409.

32
33 (10) Liu, H.; Huang, Z.; Zhao, F.; Cui, F.; Li, X.; Xia, C.; Chen, J. Efficient Hydrogenolysis of
34 Biomass-Derived Furfuryl Alcohol to 1,2- and 1,5-Pentanediols over a Non-Precious Cu-
35 Mg₃AlO_{4.5} Bifunctional Catalyst. *Catal. Sci. Technol.* **2016**, *6*, 668-671.

1
2
3 (11) Byun, J.; Han, J. An Integrated Strategy for Catalytic Co-Production of Jet Fuel Range
4 Alkenes, Tetrahydrofurfuryl Alcohol, and 1,2-Pentanediol from Lignocellulosic Biomass. *Green*
5 *Chem.* **2017**, *19*, 5214-5229.
6
7

8
9
10 (12) Ma, R.; Wu, X.-P.; Tong, T.; Shao, Z.-J.; Wang, Y.; Liu, X.; Xia, Q.; Gong, X.-Q. The
11 Critical Role of Water in the Ring Opening of Furfuryl Alcohol to 1,2-Pentanediol. *ACS Catal.*
12 **2017**, *7*, 333-337.
13
14

15
16 (13) Xu, W.; Wang, H.; Liu, X.; Ren, J.; Wang, Y.; Lu, G. Direct Catalytic Conversion of
17 Furfural to 1,5-Pentanediol by Hydrogenolysis of the Furan Ring under Mild Conditions over
18 Pt/Co₂AlO₄ Catalyst. *Chem. Commun.* **2011**, *47*, 3924-6.
19
20
21
22

23
24 (14) Sulmonetti, T. P.; Hu, B.; Lee, S.; Agrawal, P. K.; Jones, C. W. Reduced Cu-Co-Al Mixed
25 Metal Oxides for the Ring-Opening of Furfuryl Alcohol to Produce Renewable Diols. *ACS*
26 *Sustainable Chem. Eng.* **2017**, *5*, 8959-8969.
27
28
29
30

31
32 (15) Tomishige, K.; Nakagawa, Y.; Tamura, M. Selective Hydrogenolysis and Hydrogenation
33 Using Metal Catalysts Directly Modified with Metal Oxide Species. *Green Chem.* **2017**, *19*,
34 2876-2924.
35
36
37
38
39
40

41
42 (16) Giorgianni, G.; Abate, S.; Centi, G.; Perathoner, S.; van Beuzekom, S.; Soo-Tang, S.-H.;
43 Van der Waal, J. C. Effect of the Solvent in Enhancing the Selectivity to Furan Derivatives in the
44 Catalytic Hydrogenation of Furfural. *ACS Sustainable Chem. Eng.* **2018**, *6*, 16235-16247.
45
46
47
48

49
50 (17) Deng, Y.; Gao, R.; Lin, L.; Liu, T.; Wen, X.-D.; Wang, S.; Ma, D. Solvent Tunes the
51 Selectivity of Hydrogenation Reaction over α -MoC Catalyst. *J. Am. Chem. Soc.* **2018**, *140*,
52 14481-14489.
53
54
55
56
57
58
59
60

1
2
3 (18) Wu, J.; Gao, G.; Li, J.; Sun, P.; Long, X.; Li, F. Efficient and Versatile CuNi Alloy
4 Nanocatalysts for the Highly Selective Hydrogenation of Furfural. *Appl. Catal., B* **2017**, *203*,
5 227-236.
6
7

8
9
10 (19) Wang, H.; Li, X.; Lan, X.; Wang, T. Supported Ultrafine NiCo Bimetallic Alloy
11 Nanoparticles Derived from Bimetal-Organic Frameworks: A Highly Active Catalyst for
12 Furfuryl Alcohol Hydrogenation. *ACS Catal.* **2018**, *8*, 2121-2128.
13
14
15

16
17
18 (20) Chen, S.; Wojcieszak, R.; Dumeignil, F.; Marceau, E.; Royer, S. How Catalysts and
19 Experimental Conditions Determine the Selective Hydroconversion of Furfural and 5-
20 Hydroxymethylfurfural. *Chem. Rev.* **2018**, *118*, 11023-11117.
21
22
23

24
25
26 (21) Besson, M.; Gallezot, P.; Pinel, C. Conversion of Biomass into Chemicals over Metal
27 Catalysts. *Chem. Rev.* **2014**, *114*, 1827-1870.
28
29

30
31
32 (22) Mizugaki T.; Kaneda, K. Development of High Performance Heterogeneous Catalysts for
33 Selective Cleavage of C-O and C-C Bonds of Biomass-Derived Oxygenates. *Chem. Rec.* **2019**,
34 *19*, 1179-1198.
35
36
37

38
39 (23) Mizugaki, T.; Yamakawa, T.; Nagatsu, Y.; Maeno, Z.; Mitsudome, T.; Jitsukawa, K.;
40 Kaneda, K. Direct Transformation of Furfural to 1,2-Pentanediol Using a Hydrotalcite-Supported
41 Platinum Nanoparticle Catalyst. *ACS Sustainable Chem. Eng.* **2014**, *2*, 2243-2247.
42
43
44

45
46
47 (24) Zanuttini, M. S.; Gross, M.; Marchetti, G.; Querini, C. Furfural Hydrodeoxygenation on
48 Iron and Platinum Catalysts. *Appl. Catal., A*, **2019**, *587*, 117217.
49
50

51
52
53 (25) Wang, Y.; De, S.; Yan, N. Rational Control of Nano-Scale Metal-Catalysts for Biomass
54 Conversion. *Chem. Commun.* **2016**, *52*, 6210-24.
55
56
57

1
2
3 (26) Tian, S.; Gong, W.; Chen, W.; Lin, N.; Zhu, Y.; Feng, Q.; Xu, Q.; Fu, Q.; Chen, C.; Luo,
4 J.; Yan, W.; Zhao, H.; Wang, D.; Li, Y. Regulating the Catalytic Performance of Single-Atomic-
5 Site Ir Catalyst for Biomass Conversion by Metal-Support Interactions. *ACS Catal.* **2019**, *9*,
6 5223-5230.
7
8
9

10
11
12
13 (27) Lee, J.; Burt, S. P.; Carrero, C. A.; Alba-Rubio, A. C.; Ro, I.; O'Neill, B. J.; Kim, H. J.;
14 Jackson, D. H. K.; Kuech, T. F.; Hermans, I.; Dumesic, J. A.; Huber, G. W. Stabilizing Cobalt
15 Catalysts for Aqueous-Phase Reactions by Strong Metal-Support Interaction. *J. Catal.* **2015**, *330*,
16 19-27.
17
18
19
20
21

22
23 (28) Seemala, B.; Cai, C. M.; Wyman, C. E.; Christopher, P., Support Induced Control of
24 Surface Composition in Cu-Ni/TiO₂ Catalysts Enables High Yield Co-Conversion of HMF and
25 Furfural to Methylated Furans. *ACS Catal.* **2017**, *7*, 4070-4082.
26
27
28
29

30
31 (29) Liu, S.; Amada, Y.; Tamura, M.; Nakagawa, Y.; Tomishige, K. Performance and
32 Characterization of Rhenium-Modified Rh-Ir Alloy Catalyst for One-Pot Conversion of Furfural
33 into 1,5-Pentanediol. *Catal. Sci. Technol.* **2014**, *4*, 2535-2549.
34
35
36
37

38
39 (30) Meng, X.; Yang, Y.; Chen, L.; Xu, M.; Zhang, X.; Wei, M. A Control over Hydrogenation
40 Selectivity of Furfural via Tuning Exposed Facet of Ni Catalysts. *ACS Catal.* **2019**, *9*, 4226-
41 4235.
42
43
44
45

46
47 (31) Sun, Q.; Wang, S.; Liu, H. Selective Hydrogenolysis of α -C-O Bond in Biomass-Derived
48 2-Furancarboxylic Acid to 5-Hydroxyvaleric Acid on Supported Pt Catalysts at Near-Ambient
49 Temperature. *ACS Catal.* **2019**, *9*, 11413-11425.
50
51
52
53
54
55
56
57
58
59
60

1
2
3 (32) Pushkarev, V. V.; Musselwhite, N.; An, K.; Alayoglu, S.; Somorjai, G. A. High Structure
4 Sensitivity of Vapor-Phase Furfural Decarbonylation/Hydrogenation Reaction Network as A
5 Function of Size and Shape of Pt Nanoparticles. *Nano Lett.* **2012**, *12*, 5196-201.
6
7

8
9
10 (33) Rogers, S. M.; Catlow, C. R. A.; Chan-Thaw, C. E.; Chutia, A.; Jian, N.; Palmer, R. E.;
11 Perdjon, M.; Thetford, A.; Dimitratos, N.; Villa, A.; Wells, P. P. Tandem Site- and Size-
12 Controlled Pd Nanoparticles for the Directed Hydrogenation of Furfural. *ACS Catal.* **2017**, *7*,
13 2266-2274.
14
15

16
17 (34) Tong, T.; Liu, X.; Guo, Y.; Norouzi Banis, M.; Hu, Y.; Wang, Y. The Critical Role of
18 CeO₂ Crystal-Plane in Controlling Pt Chemical States on the Hydrogenolysis of Furfuryl Alcohol
19 to 1,2-Pentanediol. *J. Catal.* **2018**, *365*, 420-428.
20
21

22
23 (35) Liu, L.; Corma, A. Metal Catalysts for Heterogeneous Catalysis: From Single Atoms to
24 Nanoclusters and Nanoparticles. *Chem. Rev.* **2018**, *118*, 4981-5079.
25
26

27
28 (36) Zhang, L.; Zhou, M.; Wang, A.; Zhang, T. Selective Hydrogenation over Supported Metal
29 Catalysts: From Nanoparticles to Single Atoms. *Chem. Rev.* **2020**, *120*, 683-733.
30
31

32
33 (37) DeRita, L.; Dai, S.; Lopez-Zepeda, K.; Pham, N.; Graham, G. W.; Pan, X.; Christopher, P.
34 Catalyst Architecture for Stable Single Atom Dispersion Enables Site-Specific Spectroscopic and
35 Reactivity Measurements of CO Adsorbed to Pt Atoms, Oxidized Pt Clusters, and Metallic Pt
36 Clusters on TiO₂. *J. Am. Chem. Soc.* **2017**, *139*, 14150-14165.
37
38

39
40 (38) Zhu, Y.; An, Z.; He, J. Single-Atom and Small-Cluster Pt Induced by Sn (IV) Sites
41 Confined in an LDH Lattice for Catalytic Reforming. *J. Catal.* **2016**, *341*, 44-54.
42
43
44
45
46
47
48

1
2
3 (39) Zhu, Y.; An, Z.; Song, H.; Xiang, X.; Yan, W.; He, J. Lattice-Confined Sn (IV/II)
4 Stabilizing Raft-Like Pt Clusters: High Selectivity and Durability in Propane Dehydrogenation.
5 *ACS Catal.* **2017**, *7*, 6973-6978.
6
7

8
9
10 (40) Lang, R.; Xi, W.; Liu, J.; Cui, Y.; Li, T.; Lee, A. F.; Chen, F.; Chen, Y.; Li, L.; Li, L.; Lin,
11 J.; Miao, S.; Liu, X.; Wang, A.; Wang, X.; Luo, J.; Qiao, B.; Li, J.; Zhang, T. Non Defect-
12 Stabilized Thermally Stable Single-Atom Catalyst. *Nat. Commun.* **2019**, *10*, 234.
13
14
15

16
17 (41) Mostafa, S.; Behafarid, F.; Croy, J. R.; Ono, L. K.; Li, L.; Yang, J. C.; Frenkel, A. I.;
18 Cuenya, B. R. Shape-Dependent Catalytic Properties of Pt Nanoparticles. *J. Am. Chem. Soc.*
19 **2010**, *132*, 15714-15719.
20
21
22

23
24 (42) Panagiotopoulou, P.; Martin, N.; Vlachos, D. G. Effect of Hydrogen Donor on Liquid
25 Phase Catalytic Transfer Hydrogenation of Furfural over a Ru/RuO₂/C Catalyst. *J. Mol. Catal. A:*
26 *Chem.* **2014**, *392*, 223-228.
27
28
29

30
31 (43) Niu, B.; Luo, J.; Li, C.; Wang, B.; Liang, C. Transfer Hydrogenation of Biomass-Derived
32 Furfural to 2-Methylfuran over CuZnAl Catalysts. *Ind. Eng. Chem. Res.* **2019**, *58*, 6298-6308.
33
34
35

36
37 (44) Zhang, Z.; Yao, S.; Wang, C.; Liu, M.; Zhang, F.; Hu, X.; Chen, H.; Gou, X.; Chen, K.;
38 Zhu, Y.; Lu, X.; Ouyang, P.; Fu, J. CuZnCoO_x Multifunctional Catalyst for In Situ
39 Hydrogenation of 5-Hydroxymethylfurfural with Ethanol as Hydrogen Carrier. *J. Catal.* **2019**,
40 *373*, 314-321.
41
42
43
44

45
46 (45) Biradar, N. S.; Hengne, A. M.; Sakate, S. S.; Swami, R. K.; Rode, C. V. Single Pot
47 Transfer Hydrogenation and Aldolization of Furfural Over Metal Oxide Catalysts. *Catal. Lett.*
48 **2016**, *146*, 1611-1619.
49
50
51
52

1
2
3 (46) Koppadi, K. S.; Chada, R. R.; Enumula, S. S.; Marella, R. K.; Kamaraju, S. R. R.; Burri,
4 D. R. Metal-Free Hydrogenation of Biomass Derived Furfural into Furfuryl Alcohol Over
5 Carbon-MgO Catalysts in Continuous Mode. *Catal. Lett.* **2017**, *147*, 1278-1284.
6
7

8
9
10 (47) Koso, S.; Furikado, I.; Shima, A.; Miyazawa, T.; Kunimoria, K.; Chemoselective
11 Hydrogenolysis of Tetrahydrofurfuryl Alcohol to 1,5-Pentanediol. *Chem. Commun.* **2009**, 2035-
12 2037.
13
14
15

16
17 (48) Pouchert, C. J. *The Aldrich Library of Infrared Spectra*; Aldrich Co., Milwaukee, USA,
18 **1981**.
19
20
21

22
23 (49) Ochoa, J. V.; Trevisanut, C.; Millet, J.-M. M.; Busca, G.; Cavani, F. In Situ DRIFTS-MS
24 Study of the Anaerobic Oxidation of Ethanol over Spinel Mixed Oxides. *J. Phys. Chem. C* **2013**,
25 *117*, 23908-23918.
26
27
28

29
30 (50) Wang, F.; Shi, R.; Liu, Z.-Q.; Shang, P.-J.; Pang, X.; Shen, S.; Feng, Z.; Li, C.; Shen W.
31 Highly Efficient Dehydrogenation of Primary Aliphatic Alcohols Catalyzed by Cu Nanoparticles
32 Dispersed on Rod-Shaped La₂O₂CO₃. *ACS Catal.* **2013**, *3*, 890-894.
33
34
35
36

37
38 (51) Cattelan, L.; Perosa, A.; Riello, P.; Maschmeyer, T.; Selva, M. Continuous-Flow O-
39 Alkylation of Biobased Derivatives with Dialkyl Carbonates in the Presence of Magnesium-
40 Aluminium Hydrotalcites as Catalyst Precursors. *ChemSusChem* **2017**, *10*, 1571-1583.
41
42
43
44
45
46
47
48
49
50
51
52
53
54
55
56
57
58
59
60

1
2
3
4
5
6
7
8
9
10
11
12
13
14
15
16
17
18
19
20
21
22
23
24
25
26
27
28
29
30
31
32
33
34
35
36
37
38
39
40
41
42
43
44
45
46
47
48
49
50
51
52
53
54
55
56
57
58
59
60

Insert Table of Contents artwork here

